J Mater Sci (2011) 46:3568–3573
DOI 10.1007/s10853-011-5270-9

Micropowder injection molding: investigation of powder-binder separation using synchrotron-based microtomography and 3D image analysis

O. Weber · A. Rack · C. Redenbach · M. Schulz · O. Wirjadi

Received: 30 September 2010 / Accepted: 11 January 2011 / Published online: 29 January 2011

Abstract Micropowder injection molding (μ-PIM) is one of the most promising processes of mass production for the fabrication of small complex shaped ceramic or metallic parts with high sintered density. However, dimensional accuracy of finished parts is difficult to achieve because of extremely high shear rates during the injection molding process. This promotes the separation of powder and binder even in highly homogeneous feedstocks leading to a particle density variation in the green part causing anisotropic shrinkage during sintering. The main objective of this study is to investigate the effect of the powder particle distribution in injection molded green metallic microparts with respect to the molding parameters using synchrotron microtomography (S-μCT) and three-dimensional (3D) image evaluation. Image analysis has been performed using the MAVI software package. To get information about the allocation of the metal particles along the sample the 3D CT-scans have been segmented and statistically analyzed via spatially resolved size distributions. Furthermore, the spatial arrangement of the particles has been investigated using the so-called summary statistics from the area of point process statistics. The results show that variations in the size distribution of the metal powder particles can be detected and give consistent evidence for a monotonic increase in particle size with distance to the injection point. In order to give recommendations for the choice of parameters as well as tool construction, knowledge about the causes for separation effects is essential. This study shows that S-μCT is a well-adapted analytical tool to investigate the powder-particle distribution in μ-PIM.

O. Weber (✉) · M. Schulz
Karlsruhe Institute of Technology, Institut für Angewandte Materialien - Werkstoffprozesstechnik, Karlsruhe, Germany
e-mail: oxana.weber@kit.edu

A. Rack
European Synchrotron Radiation Facility, Grenoble, France

C. Redenbach
Department of Mathematics, TU Kaiserslautern, Kaiserslautern, Germany

O. Wirjadi
Image Processing Department, Fraunhofer ITWM, Kaiserslautern, Germany

Introduction

Micropowder injection molding (μ-PIM) allows for industry-related and low-cost production of small complex shaped ceramic or metallic microparts with high sintered density. The process combines the advantages of plastic injection molding techniques with the traditional powder metallurgy [1]. It consists of feedstock compounding from fine powder and thermoplastic polymers, shaping to a green body via μ-PIM and two post processing steps namely solvent and/or thermal debinding and sintering. These process steps have been extensively studied and are described in the literature in detail [1].

The main challenge for the production of microinjection molded parts is to achieve dimensional accuracy at the end of the process chain. Due to the multi-phase character of feedstock systems the type of processing applied can induce inhomogeneity in green parts and therefore cause inhomogeneous binder extraction or anisotropic shrinkage during sintering. This results in visual defects such as deformations, wrapping, or cracks. Most of these defects may already appear when the molding compound is injected into the cavity, because during the injection process extremely high shears rates of up to 10^6 s^{-1} [2] arise

due to the high speed and the high pressure applied. This leads to powder-binder separations or orientation effects of the powder particles in the flow direction and directly affects all following processing steps [2, 3]. Unfortunately, a direct correlation between the precursor material and the final product is often impossible. Numerous experimental tests are required to find relationships between the influence of feedstock properties and processing parameters on the mold behavior during injection molding and the quality of resulting parts. Thus, it is essential to know the particle density distribution in the molded parts to optimize the process and/or to find the parameter window most suitable for the quality expected.

In this article, the main focus is put on the phase segregation effects which are generated during the shaping step of the μ-PIM process. The influence of the machine settings on the resulting particle distribution of metal powder in the thermoplastic matrix was investigated by synchrotron microtomography (S-µCT) and the data acquired was statistically analyzed using the MAVI software package [4].

Experimental procedure and methods

Material selection and feedstock preparation

The choice of suitable powder materials for μ-PIM depends mainly on the application [2]. Major attention is paid to powders with small particle size, which should be at least about one order of magnitude smaller than the minimal dimension of the finished micropart [1]. Figure 1a shows the particle size distribution of stainless steel powder (17-4 PH, CARPENTER Technology Corp., USA) used for our research. The measurement was performed by a Microtrac X-100 laser diffraction particle size analyzer. The particle size varies from about 3 to 50 µm with an average size of 14 µm. A scanning electron microscopy (SEM) image of the metal powder is given in Fig. 1b. The majority of the particles possesses a spherical geometry close to perfection. These powder properties (large particle size, spherical shape) allow for a successful visualization of single particles by synchrotron-based X-ray microtomography and facilitate subsequent image analysis [5].

A proprietary binder system based on polyethylene and wax [6] was used for feedstock preparation. The compounding of the binder components and 63 vol% metal powder was performed at 125 °C in a kneader machine (W50 EHT, Brabender, Germany). The mixing rotation frequency was set to 30 rpm, the compounding time lasted 60 min. After compounding the material was subsequently granulated for further processing.

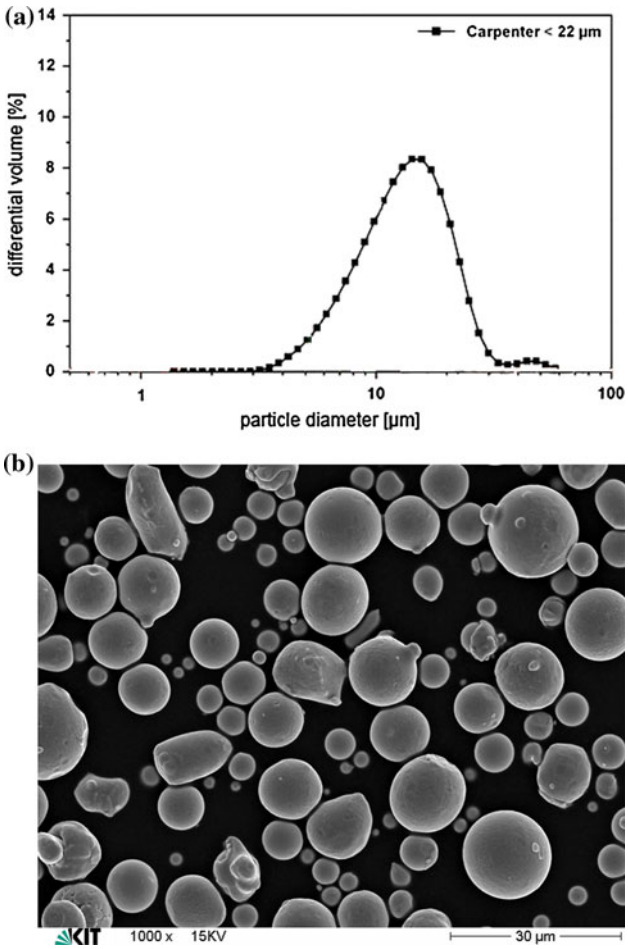

Fig. 1 **a** Particle size distribution of the stainless steel powder used (17-4 PH $d90 < 22$ µm, CARPENTER Technology Corp., USA) and **b** SEM image of the particles

Injection molding

Shaping experiments were carried out using a Microsystem 50 injection molding machine (Battenfeld GmbH, Germany) using either isothermal or variothermal process control. A flexural microspecimen geometry was chosen. In Fig. 2 a 3D model of this microstructure together with the gating system is illustrated. The bar type microstructure shows a quadratic cross section with an edge length of 260 µm and an overall length of 3250 µm (Fig. 2). An intended break is designed at the beginning of the bar type test structure that is located at the end of the flow direction. An overview of the samples studied and the corresponding injection parameters are compiled in Table 1.

Synchrotron-based X-ray microtomography

Microtomographic scans were performed at the beamline ID19 of the European Synchrotron Radiation Facility (ESRF) [7]. With respect to the available synchrotron beam

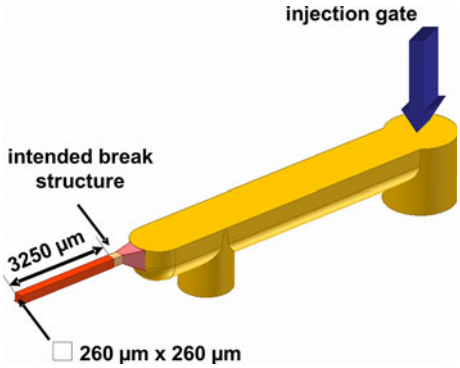

Fig. 2 3D model of the flexural microspecimen. The feedstock enters the cavity at the gating system; the investigated microstructure is located at the end of flow length

time and amount of data only one CT-scan per flexural microspecimen was prepared. Specific details about hard X-ray microtomography using laboratory-based or synchrotron light sources are published in [8, 9]. For this experiment, a high resolution indirect pixel detector as frequently used for synchrotron microimaging was employed [10]. The system consisted of a visible light microscope operating with an effective 20× magnification (NA 0.3 of the front objective) which projected the luminescence image of a 6.2-µm-thick GGG:Eu (Eu-doped $Gd_3Ga_5O_{12}$, grown on top of an undoped gadolinium gallium garnet substrate) single-crystal thin film scintillator onto the CCD chip of a FReLoN camera (type 2k14-e2v) [11, 12]. The detector operated with an effective pixel size of 0.7 µm. This resulted in a field of view of 1.4 mm and corresponds approximately to the first half of the sample length including the intended break structure. Based on the experiences from a previous experiment, the detector's corresponding resolving power is considered to be sufficient to depict the small features within the samples [5]. An X-ray photon energy of 27 keV was selected via a multilayer monochromator. 2000 projection images were recorded per 180° scan. Reconstruction of the volume images by means of filtered back-projection was performed via the ESRF software package PyHST [13, 14].

Image processing

Image processing on the reconstructed tomographic volume data sets was performed using the MAVI software package developed by the Fraunhofer ITWM [4]. The volume images were first smoothed using a 3 × 3 × 3 pixel median filter and binarized using a manually chosen, global gray value threshold. In order to separate single powder particles in the image, the watershed transform was applied to an inverted Euclidean distance map computed on the binarized volume images [15]. This well-established strategy often produces inaccurate segmentation results due to noise and artifacts in the preceding binarization step(s). Therefore, so-called pre-flooding was employed, see e.g., [15, 16], using a volume threshold of 10 pixels to prevent oversegmentation. These image processing steps are displayed in Fig. 3 using an example slice showing a cross section in the flexural specimen.

From the resulting labeled image, geometric characteristics of the single particles can be estimated using MAVI's "Object Features" [4] functionality. In the following sections, the particle volumes and 3D coordinates (centers of circumscribed cuboids) will be used. In order to remove noise and artifacts of the particle separation from the data, only those particles with a diameter larger than 3 µm will be included in all following analysis results. This is valid because it is known from the particle size distribution measurement (Fig. 1), that the smallest particles are larger than this value. In Fig. 4 the spatial arrangement of powder particles inside the investigated section of the flexural microspecimen is visualized.

In order to investigate changes in the spatial arrangement of the particles along the flow direction, each dataset was divided into ten stacks of slices, 130 µm thick each, arranged along the injection direction (Fig. 5). Within each stack, the maximal cuboid which is completely filled by material was determined such that each particle centered in the cuboid is completely contained within the image. The following statistics were computed for all particles centered in the respective cuboid ("minus sampling" [17]).

Particle size distribution

In order to measure influences of injection parameters on the spatial particle size distribution, each particle was characterized in terms of its diameter. The diameter d of a particle with volume v is computed as the diameter of an equivalent sphere with the same volume v, i.e.,

Table 1 List of the different injection molding parameters

Sample ID	Processing	Nozzle temp. (°C)	Mold temp. (°C)	Plunger velocity (mm/s)
A2, A3	Variotherm	50/45	50/45	500
A8, A9	Isotherm	45	45	500
A12	Isotherm	45	45	50

The feedstock material contained 63 vol% of metal powder in a polyethylene-wax-based binder system

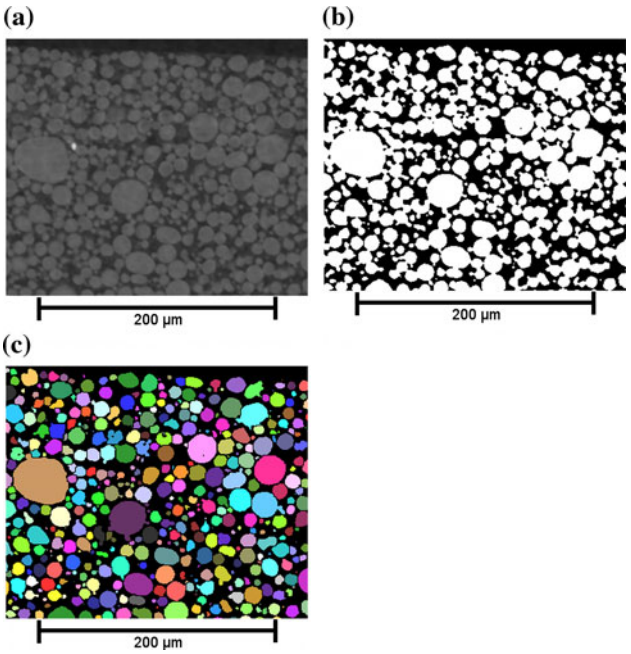

Fig. 3 Image processing steps, from left to right: **a** example slice taken from the gray-scale volume images, **b** the corresponding binarized image of the powder particles, and **c** the separated and individually labeled particles. (All processing and analysis steps were performed in 3D, 2D-slices are used for visualisation only)

$d = (6v/\pi)^{1/3}$. The mean values of the diameters in each stack are plotted in Fig. 6.

Point process statistics

For further analysis, the point patterns of particle centers in each sub-region were assumed to be realizations of a stationary and isotropic point process, i.e., invariant under translations and rotations of space. A variety of well-established summary statistics [17] to characterize such point processes is available. Here, we will only present results for the nearest-neighbor distance distribution function $G(r)$. Further summary statistics, in particular Ripley's K-function, were also applied. Since they did not provide additional information on the particle arrangement, the results are not presented here to ensure clearness.

The nearest-neighbor distance distribution function is the distribution function of the distance from a point of the point process to its nearest neighbor, i.e., $G(r)$ is the probability that the distance from a point to its nearest neighbor is smaller or equal r.

In practice, $G(r)$ is estimated from the empirical distribution function. However, edge correction techniques have to be applied since the nearest neighbor of a point might fall outside the observation window. The so-called nearest-neighbor estimator [17] which takes only points into account whose nearest neighbor is closer than the boundary of the observation window was used.

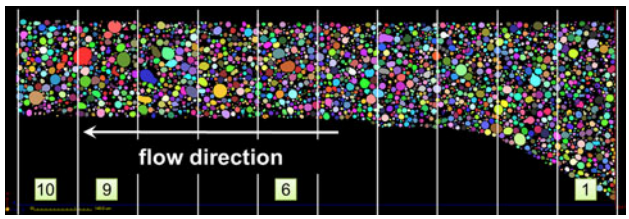

Fig. 5 Longitudinal section along the flexural microspecimen indicating the analyzed ten stacks. The distance in the flow direction between each vertical line is 130 µm, corresponding to the thickness of each stack

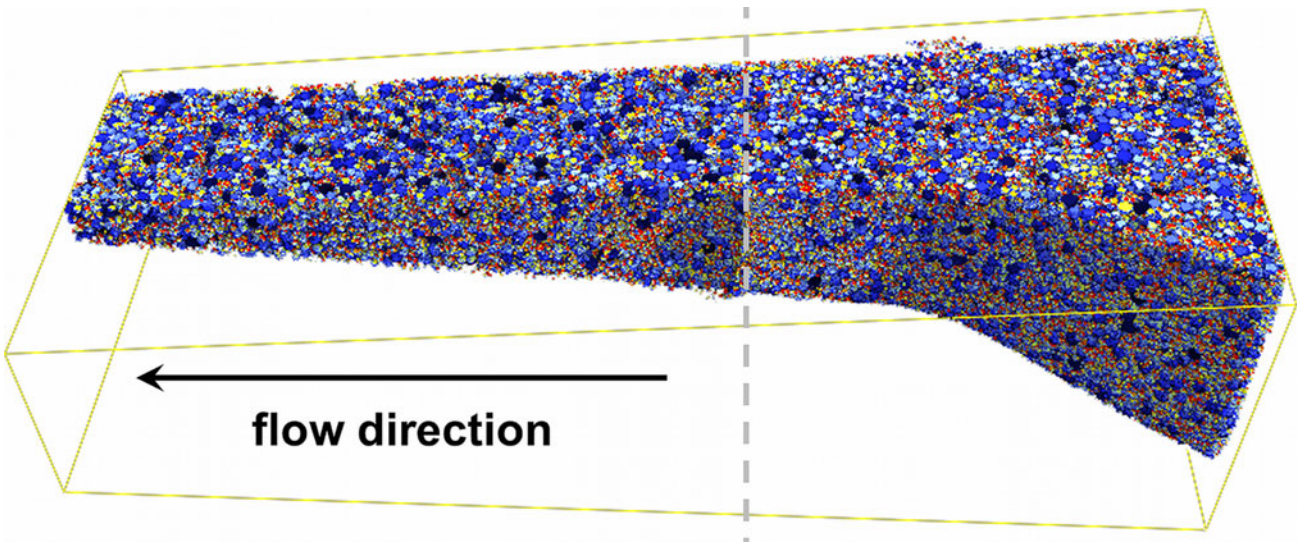

Fig. 4 Longitudinal cut through the volume data of the separated particles after image processing. The *dashed line* represents the position of the intended break. The different color values symbolize the segmentation result, similar to Fig. 3c (Color figure online)

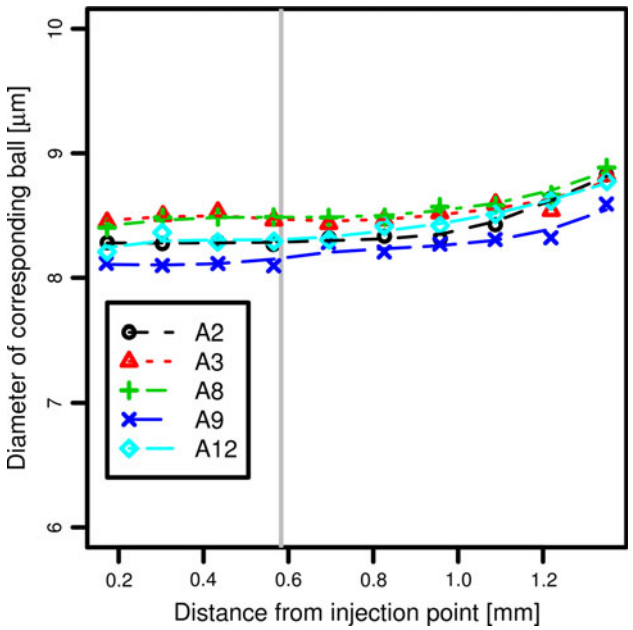

Fig. 6 Metal particle size distributions in flexural microspecimen along the flow direction: average diameter of the corresponding sphere as a function of the distance from injection gate. The *gray line* represents the position of the intended break

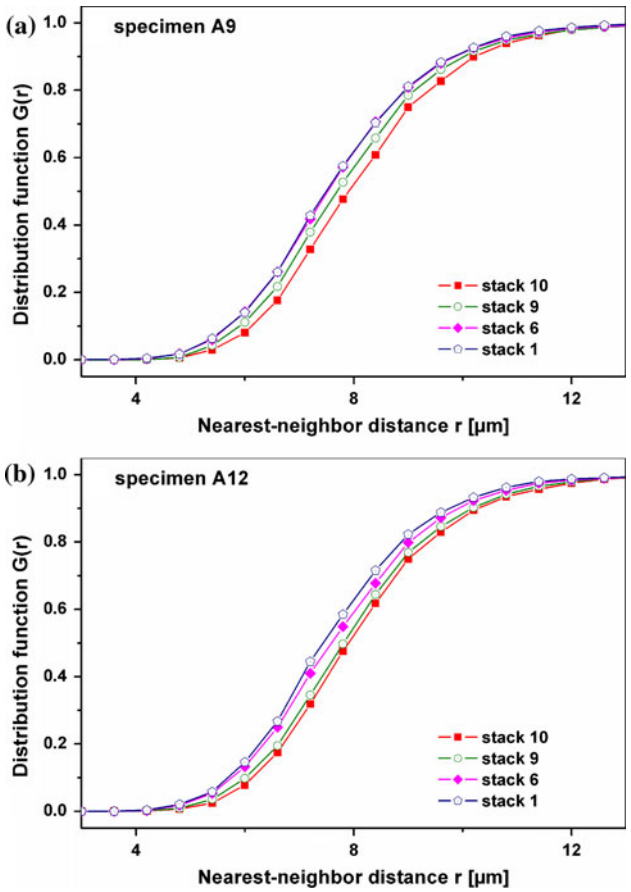

Fig. 7 Distribution functions $G(r)$ of the nearest-neighbor distance r for four selected stacks in two specimens representing different plunger velocities

The G functions for each of the ten stacks were estimated. From the trend in the particle sizes it is evident that the whole sample is not stationary. However, by subdividing the sample into sub-regions the deviation from the static state in each sub-region is small and justifies the stationarity assumption. The results are shown in Figs. 7 and 8.

Results and discussion

To determine the expected powder-binder separation, the average particle sizes were determined. The particle size distributions in all specimens are slightly increasing (Fig. 6). However, a standard deviation of ±4 µm for the analysis has to be considered.

To verify the origin of the increase in particle size, we additionally consider the nearest-neighbor distance distribution function $G(r)$ in each stack and its variation between the ten stacks. As particles do not overvlap the estimated nearest-neighbor distance distribution functions show significant deviation from complete spatial randomness toward a more regular spatial distribution (Fig. 7). The change in the summary statistics with increasing distance from the injection gate is consistent with the increase in the particle diameters observed. By considering the shift of $G(r)$ along the specimen in the flow direction the increasing trend for the particle size can be ascertained. This trend was observed in each specimen, but depending on the considered sample it was differently expressed. Figure 7 exemplarily shows the behavior of $G(r)$ for two specimens molded with different plunger velocities (Table 1).

To determine the influence of different processing parameters on the spatial particle arrangement in the defined sub-regions, the distribution functions of all specimens were compared with respect to the position. Figure 8 displays the results for four different sub-sections. Only very small differences between the specimens, i.e., different processing parameters, are detectable.

Conclusion

The results presented in this article highlight that synchrotron-based microtomography combined with 3D image analysis is a powerful analytical tool to detect and quantify powder-binder separation effects. However, concessions are necessary regarding the minimum particle size: the spatial resolution of established microtomography systems is currently not suited to resolve particle sizes below 1 µm

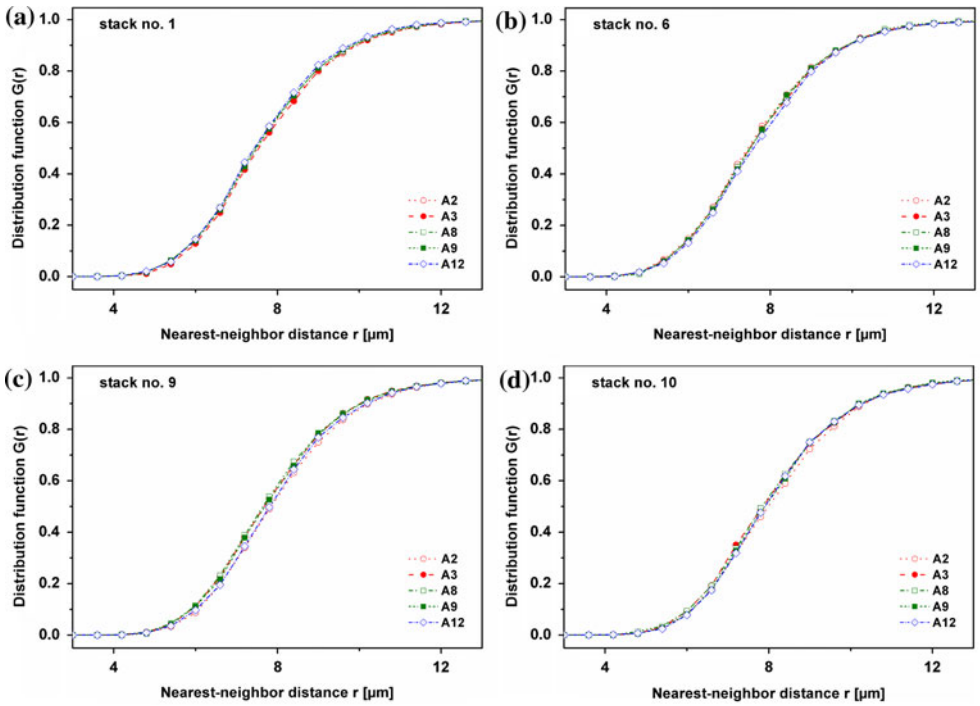

Fig. 8 Comparison of the distribution functions $G(r)$ of nearest-neighbor distance r in the specimens for four selected stacks

in combination with a field of view large enough to depict our samples. Nevertheless, variations in the size distribution of metal powder particles can be analyzed. Evidence for a monotonic increase of the particle size with the distance to the injection gate was found using the MAVI software package and confirmed by point process statistics using the nearest-neighbor distance distribution function. The S-µCT experiments presented refer to a limited section of the whole flexural microspecimen due to limitations introduced by the amount of data and available synchrotron beam time. In future studies, the complete flow length will be investigated. This is required to optimize the ratio between the values for the particle size which increase in the flow direction and the standard deviation of the distribution in each stack. In addition, the particle size and particle density distribution perpendicular to the flow direction and the density distribution along the flow direction are currently under investigation.

This article presents the first step for defining a measurement procedure. The final aim of the research activities are guidelines for tool construction and the choice of parameters for the production of defect free, dense microparts produced by powder-injection molding.

Acknowledgements The authors would like to acknowledge Elodie Boller (ESRF) for her support at the beamline ID19 and the colleagues from KIT for doing the μ-PIM experiments. Financial support by the Deutsche Forschungsgemeinschaft (DFG, German Research Foundation) in the framework of the Collaborate Research Project SFB499 is greatly acknowledged.

References

1. German RM (1990) Powder injection moulding. Metal Powder Industries Federation, Princeton
2. Heldele R, Rath S, Merz L, Butzbach R, Hagelstein M, Hausselt J (2006) Nucl Instrum & Meth Phys Res B 246:211
3. Gelin JC, Barriere T, Song J (2010) J Eng Mater Technol 132:011017
4. MAVI—Modular Algorithms for Volume Images (2010) Fraunhofer ITWM, Department of Image Processing, Kaiserslautern. http://www.mavi-3d.de. Accessed 25 Jan 2011
5. Rack A, Weitkamp T, Trabelsi SB, Modregger P, Cecilia A et al (2009) Nucl Instrum & Meth Phys Res B 267:1978
6. Heldele R (2008) Adv Powder Metall Part Mater IV(Part 11)
7. Weitkamp T, Tafforeau P, Boller E, Cloetens P, Valade JP et al (2010) AIP Conf Proc 1221:33
8. Banhart J (2008) Advanced tomographic methods in materials research and engineering. Oxford University Press, Oxford
9. Stock SR (2008) Microcomputed tomography: methodology and applications. CRC Press, London
10. Koch A, Raven C, Spanne P, Snigirev A (1998) J Opt Soc Am A 15:1940
11. Martin T, Koch A (2006) J Synchrotron Rad 13:180
12. Labiche JC, Mathon O, Pascarelli S et al (2007) Rev Sci Instrum 78:0901301
13. Mirone A, Wilcke R, Hammersley A, Ferrero C (2010). http://www.esrf.eu/UsersAndScience/Experiments/TBS/SciSoft/. Accessed 20 Jan 2011
14. Kak AC, Slaney M (1988) Principles of computerized tomographic imaging. IEEE Press, New York
15. Ohser J, Schladitz K (2009) 3D images of materials structures—processing and analysis. Wiley-VCH, Weinheim
16. Tek FB, Dempster AG, Kale I (2005) Comp Imag Vis 30:441
17. Illian J (2008) Statistical analysis and modelling of spatial point patterns. Wiley, Chichester